Superradiant Phase Transition in a Superconducting Circuit in Thermal Equilibrium

Motoaki Bamba,[1,*] Kunihiro Inomata,[2] and Yasunobu Nakamura[2,3]
[1]Department of Materials Engineering Science, Osaka University, 1-3 Machikaneyama, Toyonaka, Osaka 560-8531, Japan
[2]RIKEN Center for Emergent Matter Science (CEMS), 2-1 Hirosawa, Wako, Saitama 351-0198, Japan
[3]Research Center for Advanced Science and Technology (RCAST), University of Tokyo, Meguro-ku, Tokyo 153-8904, Japan
(Received 3 May 2016; published 20 October 2016)

We propose a superconducting circuit that shows a superradiant phase transition (SRPT) in thermal equilibrium. The existence of the SRPT is confirmed analytically in the limit of an infinite number of artificial atoms. We also perform a numerical diagonalization of the Hamiltonian with a finite number of atoms and observe an asymptotic behavior approaching the infinite limit as the number of atoms increases. The SRPT can also be interpreted intuitively in a classical analysis.

DOI: 10.1103/PhysRevLett.117.173601

In a variety of studies involving the light-matter interaction, the realization of a superradiant phase transition (SRPT) still remains a challenging subject. This refers to the spontaneous appearance of the coherence amplitude of transverse electromagnetic fields due to the light-matter interaction in the thermal equilibrium. Though the laser also shows the spontaneous coherence, it is generated by population-inverted matters, i.e., in a nonequilibrium situation. The SRPT was first proposed theoretically around 1970 [1–3], but later its absence in the thermal equilibrium was pointed out based on the so-called A^2 term [4–7] and, more generally, on the minimal-coupling Hamiltonian [8,9]. A SRPT analogue in nonequilibrium situations was proposed theoretically [10] and was observed experimentally in cold atoms driven by laser light [11,12]. Realizing a thermal-equilibrium SRPT and comparing it with the nonequilibrium SRPT (including a laser) are fundamental subjects bridging statistical physics (or thermodynamics), established in equilibrium situations, and electrodynamics (or the light-matter interaction), which has been long discussed mostly in nonequilibrium situations. However, the SRPT has not yet been realized in the thermal equilibrium since the first proposal [1–3].

While the atomic systems are basically described by the minimal-coupling Hamiltonian [8,9], there are a large number of degrees of freedom in designing the Hamiltonians of superconducting circuits, where the existence of the SRPT is still under debate [13–16]. In this Letter, we propose the superconducting circuit depicted in Fig. 1. We derive the Hamiltonian of this circuit by the standard quantization procedure [17] as in the recent work which showed the absence of SRPT in a different circuit structure [16]. We examine its existence in our circuit by using the semiclassical approach [3,8,9,18,19], which is known to be justified in the thermodynamic limit (with an infinite number of atoms), as well as by straightforwardly diagonalizing the Hamiltonian with a finite number of atoms.

The circuit shown in Fig. 1 has a LC resonator with capacitance C_R and inductance L_R, coupled to N parallel branches containing a Josephson junction. Each junction has Josephson energy E_J and shunt capacitance C_J and is connected to the LC resonator through inductance L_g individually. This configuration is distinct from the conventional inductive [16,20] and capacitive [16] couplings, where the existence of the SRPT was proposed [13,15] but later denied [14,16]. However, the no-go result was shown only for specific configurations [14,16] and is not applied to ours. We first explain why the SRPT occurs in our circuit by analyzing the form of the Hamiltonian.

We apply a static external flux bias $\Phi_{\rm ext} = \Phi_0/2$ in the loop between the resonator and the junctions, where $\Phi_0 = h/(2e)$ is the flux quantum. Alternatively, we can remove the external field and replace the Josephson junctions with π junctions, which have an inverted energy-phase relation [21]. We define the ground and the branch fluxes ϕ and $\{\psi_j\}$ $(j = 1, \ldots, N)$ as in Fig. 1. According to the flux-based procedure [17], the Hamiltonian is derived straightforwardly and quantized as

$$\hat{H} = \frac{\hat{q}^2}{2C_R} + \frac{\hat{\phi}^2}{2L_R} + \sum_{j=1}^{N}\left(\frac{\hat{\rho}_j{}^2}{2C_J} + \frac{(\hat{\psi}_j - \hat{\phi})^2}{2L_g} + E_J \cos\frac{2\pi\hat{\psi}_j}{\Phi_0}\right). \tag{1}$$

Here, $\hat{q}$ and $\{\hat{\rho}_j\}$ are the conjugate momenta of $\hat{\phi}$ and $\{\hat{\psi}_j\}$, respectively, satisfying $[\hat{\phi}, \hat{q}] = i\hbar$ and $[\hat{\psi}_j, \hat{\rho}_{j'}] = i\hbar\delta_{j,j'}$.

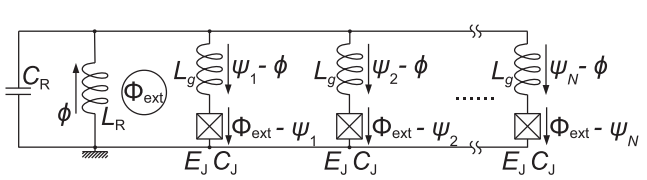

FIG. 1. Superconducting circuit showing the SRPT in thermal equilibrium under a static external magnetic flux bias $\Phi_{\rm ext} = \Phi_0/2$.

 © 2016 American Physical Society

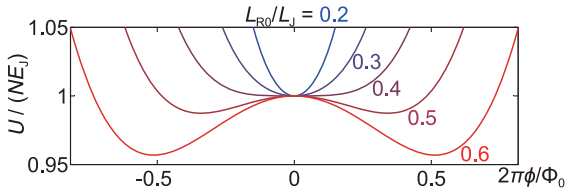

FIG. 2. Normalized inductive energy [Eq. (2)] versus $2\pi\phi/\Phi_0$ under the condition of $\psi_j = (1 + L_g/L_{R0})\phi$, which is obtained by $\partial U/\partial\phi = 0$. For $NL_R = L_{R0} > L_J - L_g$, the inductive energy shows two minima at $\phi \neq 0$. This transition corresponds to the SRPT in the sense of the quantum phase transition. The parameter is $L_g = 0.6L_J$.

Let us first understand intuitively the SRPT in our circuit by a classical analysis. The inductive energy in Eq. (1) is extracted as

$$U(\phi, \{\psi_j\}) = \frac{\phi^2}{2L_R} + \sum_{j=1}^{N}\left(\frac{(\psi_j - \phi)^2}{2L_g} + E_J \cos\frac{2\pi\psi_j}{\Phi_0}\right). \quad (2)$$

The energy minima correspond to the ground state in the classical physics. Though the parabolic terms $\phi^2/(2L_R)$ and $(\psi_j - \phi)^2/(2L_g)$ are minimized at $\phi = \psi_j = 0$, the anharmonic term $E_J \cos(2\pi\psi_j/\Phi_0)$ is minimized at $\psi_j = \pm\Phi_0/2$. This is owing to the external flux bias $\Phi_{\rm ext} = \Phi_0/2$; the sign of the last term in Eqs. (1) and (2) is positive, because the phase difference across the Josephson junction is given by $\pi - 2\pi(\psi_j/\Phi_0)$ due to the flux quantization in each loop consisting of L_R, L_g, and the junction. This competition between the parabolic and anharmonic inductive energies is the trick for realizing the SRPT.

In order to simplify the following discussion, we define an inductance $L_J \equiv [\Phi_0/(2\pi)]^2/E_J$ by the Josephson energy E_J. The inductive energy U in Eq. (2) is minimized for $\psi_j = [1 + L_g/(NL_R)]\phi$, which is obtained from $\partial U/\partial\phi = 0$. Because the SRPT is basically discussed in the thermodynamic limit $N \to \infty$, we scale the inductance of the LC resonator by the number N of junctions as $L_R = L_{R0}/N$, where L_{R0} is N-independent inductance. Then, the inductive energy U/N per junction becomes independent of N. In Fig. 2, we plot $U/(NE_J)$ as a function of $2\pi\phi/\Phi_0$ under the condition of $\psi_j = (1 + L_g/L_{R0})\phi$. The five curves in Fig. 2 are the results for different L_{R0} under a fixed L_g of $0.6L_J$. The inductive energy U is minimized at $\phi = \psi_j = 0$ for $L_{R0} < L_J - L_g = 0.4L_J$, because the parabolic terms dominate. In contrast, the anharmonic term dominates when L_{R0} satisfies

$$NL_R = L_{R0} > L_J - L_g. \quad (3)$$

Then, U is minimized at the two points with nonzero fluxes $\phi = \pm\phi_0$. In quantum theory, the real ground state is a superposition of the two minimum points [conceptually speaking, $|g\rangle = (|\phi_0\rangle + |-\phi_0\rangle)/\sqrt{2}$] and the expectation values of the fluxes are zero $\langle g|\hat{\phi}|g\rangle = \langle g|\hat{\psi}_j|g\rangle = 0$ for finite N. However, the thermodynamic limit $N \to \infty$ justifies the classical approach, because the height of the potential barrier in the whole system is proportional to N. Then, in this limit, we find a spontaneous appearance of coherence (symmetry breaking); i.e., nonzero $\phi = \pm\phi_0$ and $\psi_j = \pm(1 + L_g/L_{R0})\phi_0$ appear in the circuit. This transition from $\phi = 0$ to $\pm\phi_0$ by changing L_{R0} corresponds to the SRPT in the sense of the quantum phase transition [22,23], as discussed below in a quantum analysis.

Let us compare Eq. (1) with the minimal-coupling Hamiltonian (under the long-wavelength approximation as discussed in Ref. [8])

$$\hat{H}_{\rm min} = \hat{H}_{\rm em} + \sum_{j}^{N}\frac{(\hat{p}_j - e\hat{A})^2}{2m} + \hat{V}(\{\hat{x}_j\}). \quad (4)$$

Here, $\hat{H}_{\rm em}$ represents the energy of the transverse electromagnetic fields described by the vector potential $\hat{A}$ and its conjugate momentum. The second and the last terms are, respectively, the kinetic and the Coulomb interaction energies of particles with mass m, charge e, and momentum $\{\hat{p}_j\}$ at position $\{\hat{x}_j\}$. The kinetic energy $(\hat{p}_j - e\hat{A})^2/(2m)$ corresponds to the inductive one $(\hat{\psi}_j - \hat{\phi})^2/(2L_g)$ at L_g in Eq. (1). In this way, $\hat{\psi}_j$ and $\hat{\phi}$ correspond to $\hat{p}_j$ and $\hat{A}$, respectively, and then $\hat{\rho}_j$ corresponds to $\hat{x}_j$. The no-go theorem of the SRPT in the minimal-coupling Hamiltonian relies on the fact that the mixing term $(\hat{p}_j - e\hat{A})^2/(2m)$ and the anharmonic term $\hat{V}(\{\hat{x}_j\})$ are, respectively, described by $\hat{p}_j$ and $\hat{x}_j$ [8,9]. In contrast, in our Hamiltonian, Eq. (1), both the mixing $(\hat{\psi}_j - \hat{\phi})^2/(2L_g)$ and the anharmonicity $E_J \cos(2\pi\hat{\psi}_j/\Phi_0)$ are described by $\hat{\psi}_j$. This is the essence for avoiding the no-go theorem [8,9] and also for the transition discussed in the above classical analysis. In the Supplemental Material [24], we also explain how we avoid the no-go results based on the A^2 [4–7] and the P^2 [27,28] terms. The latter corresponds to the direct qubit-qubit interaction discussed recently in Ref. [16].

By decomposing $\sum_{j=1}^{N}(\hat{\psi}_j - \hat{\phi})^2/(2L_g)$ in Eq. (1), we obtain $N\hat{\phi}^2/(2L_g)$. This corresponds to the A^2 term [4,5] (since $\hat{\phi}$ corresponds to $\hat{A}$) and renormalizes the frequency of the LC resonator as $\omega_c = \sqrt{(N/L_g + 1/L_R)/C_R}$. Here, in order to make ω_c independent of N, in addition to the scaling $L_R = L_{R0}/N$, we also scale the capacitance as $C_R = NC_{R0}$, where C_{R0} is N-independent capacitance. Introducing an annihilation operator $\hat{a} \equiv \hat{\phi}/\sqrt{2\hbar Z_c} + i\hat{q}\sqrt{Z_c/(2\hbar)}$, where the impedance Z_c is scaled as $Z_c = Z_{c0}/N$ for $Z_{c0} = \sqrt{(1/L_g + 1/L_{R0})^{-1}/C_{R0}}$, the Hamiltonian in Eq. (1) is rewritten as

$$\hat{H} = \hbar\omega_c\left(\hat{a}^\dagger\hat{a} + \frac{1}{2}\right) - \frac{\hat{\phi}}{L_g}\sum_{j=1}^{N}\hat{\psi}_j + \sum_{j=1}^{N}\hat{H}_j^{\rm atom}. \quad (5)$$

Here, the Hamiltonian involving the jth junction is

$$\hat{H}_j^{\rm atom} = \frac{\hat{\rho}_j^{\,2}}{2C_J} + \frac{\hat{\psi}_j^{\,2}}{2L_g} + E_J \cos\frac{2\pi\hat{\psi}_j}{\Phi_0}. \tag{6}$$

Although we cannot obtain $\hat{H}_j^{\rm atom}$ by simply extracting a part of elements from the circuit in Fig. 1, this anharmonic oscillator described by $\hat{\psi}_j$ and $\hat{\rho}_j$ is formally considered to be our "atom." The first term in Eq. (5) is the Hamiltonian of our "photons," which is described by $\hat{\phi}$ and $\hat{q}$ or $\hat{a}$, renormalized by the A^2 term. The second term in Eq. (5) is our "photon-atom interaction." In the following, we discuss the SRPT in terms of these photons and atoms in relation to previous discussions on the Dicke model [1–3,13,15,22,23].

In contrast to the two-level atoms considered in the Dicke model, our atoms have weakly nonlinear bosonic transitions (we explain in detail the parameters used in the following calculations in the Supplemental Material [24]). In Fig. 3(b), the solid curve represents the atomic wave function at each atomic level, which are calculated from $\hat{H}_j^{\rm atom}$ in Eq. (6). The dashed curve represents the inductive energy as a function of $2\pi\psi_j/\Phi_0$. In this Letter, we basically consider the case $L_J > L_g = 0.6L_J$. Then, since the anharmonic energy $E_J\cos(2\pi\psi_j/\Phi_0)$ is smaller than the parabolic one $\psi_j^{\,2}/(2L_g)$, as seen in Fig. 3(b), the inductive energy in each atom is minimized at $\psi_j = 0$, and the nonlinearity is only about 3%.

Here, we tentatively neglect the anharmonicity as $E_J\cos(2\pi\hat{\psi}_j/\Phi_0) \simeq E_J - \hat{\psi}_j^{\,2}/(2L_J)$ and assume that the transitions in each atom are described approximately by bosonic annihilation operator $\hat{b}_j = \hat{\psi}_j/\sqrt{2\hbar Z_a} + i\hat{\rho}_j\sqrt{Z_a/(2\hbar)}$ as

$$\hat{H} \simeq \hbar\omega_c\left(\hat{a}^\dagger\hat{a} + \frac{1}{2}\right) + \sum_{j=1}^{N}\hbar\omega_a\left(\hat{b}_j^\dagger\hat{b}_j + \frac{1}{2}\right) - \frac{\hbar g}{\sqrt{N}}(\hat{a} + \hat{a}^\dagger)\sum_{j=1}^{N}(\hat{b}_j + \hat{b}_j^\dagger) + NE_J. \tag{7}$$

Here, $\omega_a = \sqrt{(1/L_g - 1/L_J)/C_J}$ is the atomic transition frequency, and the interaction strength g is expressed as $g = \sqrt{NZ_cZ_a}/(2L_g) = \sqrt{Z_{c0}Z_a}/(2L_g)$, where we define another impedance $Z_a = \sqrt{(1/L_g - 1/L_J)^{-1}/C_J}$.

Two transition frequencies $\omega_\pm$ of the bosonized Hamiltonian in Eq. (7) are obtained easily by the Bogoliubov transformation [29,30] as

$$\omega_\pm^{\,2} = \frac{\omega_c^{\,2} + \omega_a^{\,2} \pm \sqrt{(\omega_c^{\,2} - \omega_a^{\,2})^2 + 16g^2\omega_c\omega_a}}{2}. \tag{8}$$

Note that ω_c, ω_a, g, and $\omega_\pm$ are not scaled with N by the scaling $L_R = L_{R0}/N$ and $C_R = NC_{R0}$. The expression in Eq. (8) is exactly the same as the one derived in the Holstein-Primakoff approach for the Dicke model [22,23]. When ω_- becomes imaginary, the normal ground state (showing $\langle g|\hat{a}|g\rangle = \langle g|\hat{\phi}|g\rangle = 0$) becomes unstable. However, it is an artifact due to the neglect of the anharmonicity in Eq. (7). As found in the classical analysis in Fig. 2, the real ground state appears at an inductive energy minimum with $\phi = \pm\phi_0$ (superradiant ground state with a photonic amplitude of $\langle g|\hat{a}|g\rangle \simeq \pm\phi_0/\sqrt{2\hbar Z_c}$) in the presence of the anharmonicity [6,7,22,23,31]. Equation (8) suggests that the superradiant ground state appears for $4g^2 > \omega_c\omega_a$, which gives exactly the same condition as Eq. (3) obtained by the classical approach. While these conditions are certainly satisfied in our circuit, we will obtain a more rigorous condition of the SRPT in the following semiclassical analysis.

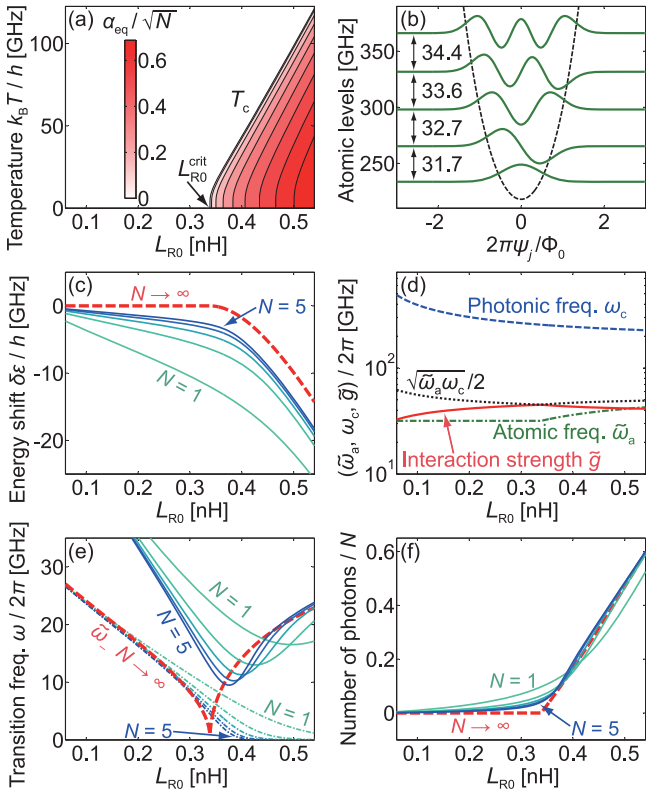

FIG. 3. (a) Normalized photonic amplitude $\alpha_{\rm eq}/\sqrt{N}$ in the thermodynamic limit (infinite number of atoms $N\to\infty$) versus $L_{R0} = NL_R$ and temperature k_BT/h in frequency units. The SRPT occurs at $L_{R0}^{\rm crit}$ at $T = 0$. (b) Atomic levels, potential, and wave functions. (c) Zero-point energy shift, (e) transition frequency, and (f) number of photons per atom versus L_{R0}. Dashed curves are obtained in the thermodynamic limit, and solid curves are calculated for $N = 1,\ldots,5$. In panel (e), the dash-dotted curves represent the transition frequencies for exciting an odd number of bosons, while the solid curves are those for exciting an even number of bosons. (d) Photonic frequency ω_c, renormalized atomic frequency $\tilde{\omega}_a$, and renormalized light-matter interaction strength $\tilde{g}$ versus L_{R0}. The SRPT occurs when $\tilde{g}$ reaches the critical interaction strength $\sqrt{\tilde{\omega}_a\omega_c}/2$ plotted by the dotted line. The parameters are $L_J = 0.75$ nH, $L_g = 0.6L_J = 0.45$ nH, $C_J = 24$ fF, and $C_{R0} = 2$ fF $= C_R/N$.

The above classical and bosonic quantum analyses imply the SRPT in the sense of the quantum phase transition, i.e., in the limit of $T\to 0$. For finite temperature $T \geq 0$, we calculate the photonic amplitude $\alpha_{\rm eq}$ by the partition

function $\mathcal{Z}(T) = \mathrm{Tr}[e^{-\hat{H}/k_BT}]$ in the semiclassical analysis [3,8,9,18,19] (see the Supplemental Material [24]).

In Fig. 3(a), the normalized photonic amplitude $\alpha_{\rm eq}/\sqrt{N}$ is color plotted as a function of the inductance $L_{R0} = NL_R$ and temperature k_BT/h in frequency units. What is important is the ratio of the inductances. The Josephson inductance is assumed to be $L_J = [\Phi_0/(2\pi)]^2/E_J = 0.75$nH, and the connecting inductance $L_g = 0.6L_J = 0.45$ nH. At $T = 0$, the nonzero photonic amplitude $\alpha_{\rm eq}$ appears for $L_{R0} > L_{R0}^{\rm crit} \simeq 0.34$ nH, which roughly agrees with the classical result $L_J - L_g = 0.30$ nH in Eq. (3). The deviation is due to the quantum treatment of atoms in the semiclassical analysis. The photonic flux $\phi_{\rm eq} = \sqrt{2\hbar Z_{c0}}\alpha_{\rm eq}/\sqrt{N}$ roughly agrees with ϕ_0 giving the minimum of the inductive energy U in Eq. (2) in the classical analysis. The nonzero $\alpha_{\rm eq}$ and $\phi_{\rm eq}$ appear even at finite temperatures, and the critical temperature T_c increases with increasing L_{R0}. This is the main evidence of the thermal-equilibrium SRPT in our circuit, which is obtained in the thermodynamic limit $N \to \infty$.

The transition frequencies, which are experimentally observable, are obtained by quantizing the fluctuation around the equilibrium values of the fluxes $\phi_{\rm eq}$ and $\psi_{\rm eq}$ determined in the semiclassical approach [24]. A similar analysis has been performed in Refs. [22,23] for the Dicke Hamiltonian. At $T = 0$, the original Hamiltonian in Eq. (1) is expanded with respect to the fluctuations $\delta\hat{\phi} = \hat{\phi} - \phi_{\rm eq}$ and $\delta\hat{\psi}_j = \hat{\psi}_j - \psi_{\rm eq}$ up to $O(\delta\hat{\psi}_j{}^2)$ [24] as

$$\hat{H} \simeq \frac{\hat{q}^2}{2C_R} + \frac{\delta\hat{\phi}^2}{2L_R} + \sum_{j=1}^{N}\left\{\frac{\hat{\rho}^2}{2C_J} + \frac{(\delta\hat{\phi} - \delta\hat{\psi}_j)^2}{2L_g} - \frac{\delta\hat{\psi}_j{}^2}{2\tilde{L}_J}\right\} + N(E_J + \delta\varepsilon). \quad (9)$$

Here, $\tilde{E}_J = E_J\langle\cos(2\pi\hat{\psi}/\Phi_0)\rangle_{\rm g}^{\rm eff}$ and $\tilde{L}_J = [\Phi_0/(2\pi)]^2/\tilde{E}_J$ are calculated by an effective Hamiltonian in the semiclassical approach [24] and are modified by the quantum treatment of atoms even before the SRPT. The zero-point energy shift per atom is $\delta\varepsilon = \phi_{\rm eq}{}^2/(2L_{R0}) + (\phi_{\rm eq} - \psi_{\rm eq})^2/(2L_g) + \tilde{E}_J - E_J$. This shift $\delta\varepsilon/h$ is plotted as the dashed curve in Fig. 3(c). After the appearance of nonzero amplitudes $\phi_{\rm eq}$ and $\psi_{\rm eq}$, the zero-point energy is decreased by the light-matter interaction.

The transition frequencies $\tilde{\omega}_\pm$ are calculated also from Eq. (8) but by replacing ω_a and g by $\tilde{\omega}_a = [(1/L_g - 1/\tilde{L}_J)/C_J]^{1/2}$ and $\tilde{g} = [Z_{c0}\tilde{Z}_a]^{1/2}/(2L_g)$, respectively, where $\tilde{Z}_a = [(1/L_g - 1/\tilde{L}_J)^{-1}/C_J]^{1/2}$. $\tilde{\omega}_a$, ω_c, and $\tilde{g}$ are plotted in Fig. 3(d). When $\tilde{g}$ reaches the critical value $\sqrt{\tilde{\omega}_a\omega_c}/2$ plotted by the dotted line, the SRPT occurs. Compared with the simple condition $4g^2 > \omega_c\omega_a$ (giving the critical inductance $L_J - L_g = 0.30$ nH) obtained from Eq. (7) under the bosonic approximation, the deviation is due to the consideration of the anharmonicity in Eq. (9). The lower transition frequency $\tilde{\omega}_-$ is plotted by the dashed line in Fig. 3(e). It never becomes of imaginary value but shows a cusp at $L_{R0}^{\rm crit}$. In contrast to the Dicke model [22,23], $\tilde{\omega}_-$ does not become zero even at $L_{R0}^{\rm crit}$ in our system. It is due to the presence of multiple atomic levels with anharmonicity (our atom cannot be equivalent with the two-level limit because $L_J > L_g$ is required). On the other hand, in the limit of negligible anharmonicity ($L_J \gg L_g$), the SRPT condition in Eq. (3) is justified, and $\tilde{\omega}_-$ drops to zero at $L_{R0}^{\rm crit}$.

Here, we note that, in the limit of $L_g \to 0$, we definitively obtain $\psi_j = \phi$, as seen in Eq. (1) or in the circuit of Fig. 1, while the transition in Fig. 2 itself occurs in the classical approach. We also obtain $\omega_a, g \to \infty$, while $4g^2 > \omega_c\omega_a$ is reduced to $L_{R0} > L_J$, and the transition still remains. However, in order to distinguish the photons and atoms and to discuss the SRPT, we need a finite L_g; this is especially because, as far as we checked numerically, L_{R0}, L_J, and L_g are desired to be in the same order to observe a sharp drop of the transition frequency for finite N, as we will see in the following.

In addition to the above semiclassical approach justified in the thermodynamic limit $N \to \infty$, we also diagonalize numerically the original Hamiltonian in Eq. (5) for $N = 1, 2, \ldots, 5$ in order to predict the tendency to be observed in experiments with a finite number of junctions. To express the Hamiltonian with a sparse matrix and reduce the computational cost, we expand $\cos(2\pi\hat{\psi}_j/\Phi_0)$ and consider the terms up to $O(\hat{\psi}_j{}^4)$ (see the details of the numerical diagonalization in the Supplemental Material [24]).

Because the total Hamiltonian in Eqs. (1) or (5) has parity symmetry, the expectation value of the photonic amplitude in the ground state is basically zero for finite N. The nonzero $\alpha_{\rm eq}$ is obtained only in the thermodynamic limit $N \to \infty$. In the numerical diagonalization of the Hamiltonian, we first consider the subsystem with even numbers of bosons as in Ref. [23], because it is not mixed with the other subsystem with odd numbers of bosons. For the obtained ground state $|g\rangle$ with an energy E_g, the expectation number of photons $\langle g|\hat{a}^\dagger\hat{a}|g\rangle/N$ per atom is plotted in Fig. 3(f) for $N = 1, \ldots, 5$. The dashed curve shows $\alpha_{\rm eq}{}^2/N$ in the thermodynamic limit. Figure 3(c) shows the zero-point energy shift $\delta\varepsilon = (E_g - \hbar\omega_c/2)/N - \varepsilon_{a0}$ per atom, where ε_{a0} is the atomic zero-point energy seen in Fig. 3(b). The transition frequency from the ground state to the first excited state in the even-number subsystem is plotted as solid curves in Fig. 3(e). It sharply drops around $L_{R0}^{\rm crit}$ even with $N = 5$ atoms and asymptotically reproduces the thermodynamic limit (dashed curve) for $L_{R0} > L_{R0}^{\rm crit}$. On the other hand, the dash-dotted curves represent the transition frequency from the ground state to the lowest state in the odd-number subsystem. They asymptotically approach the thermodynamic limit for $L_{R0} < L_{R0}^{\rm crit}$ and vanish for $L_{R0} > L_{R0}^{\rm crit}$, as seen also in Refs. [20,23]. These characteristic features imply the existence of the SRPT, i.e., the parity symmetry breaking [22,23].

We conclude that the superconducting circuit in Fig. 1 shows the SRPT in the thermal equilibrium. It was

confirmed by the semiclassical approach in the thermodynamic limit. It was also checked by calculating the number of photons, transition frequency, and zero-point energy shift in the numerical diagonalization of the Hamiltonian with a finite number of atoms. Experimentally, the transition frequency could be observed by measuring the excitation spectra, which would reveal a drastic behavior around the critical point, as seen in Fig. 3(e), by changing L_{R0}, by decreasing the temperature, or by increasing the number of atoms.

We thank P.-M. Billangeon for fruitful discussions. M. B. also thanks F. Yoshihara for critical comments. This work was funded by ImPACT Program of Council for Science, Technology and Innovation (Cabinet Office, Government of Japan) and by JSPS KAKENHI (Grants No. 26287087, No. 26220601, and No. 15K17731).

*bamba@qi.mp.es.osaka-u.ac.jp

[1] W. R. Mallory, Solution of a Multiatom Radiation Model Using the Bargmann Realization of the Radiation Field, Phys. Rev. **188**, 1976 (1969).
[2] K. Hepp and E. H. Lieb, On the superradiant phase transition for molecules in a quantized radiation field: The Dicke maser model, Ann. Phys. (N.Y.) **76**, 360 (1973).
[3] Y. K. Wang and F. T. Hioe, Phase Transition in the Dicke Model of Superradiance, Phys. Rev. A **7**, 831 (1973).
[4] K. Rzążewski, K. Wódkiewicz, and W. Żakowicz, Phase Transitions, Two-Level Atoms, and the A^2 Term, Phys. Rev. Lett. **35**, 432 (1975).
[5] K. Rzążewski and K. Wódkiewicz, Thermodynamics of two-level atoms interacting with the continuum of electromagnetic field modes, Phys. Rev. A **13**, 1967 (1976).
[6] M. Yamanoi, Influence of omitting the A^2 term in the conventional photon-matter-Hamiltonian on the photon-field equation, Phys. Lett. **58A**, 437 (1976).
[7] M. Yamanoi, On polariton instability and thermodynamic phase transition in a photon-matter system, J. Phys. A **12**, 1591 (1979).
[8] I. Bialynicki-Birula and K. Rzążewski, No-go theorem concerning the superradiant phase transition in atomic systems, Phys. Rev. A **19**, 301 (1979).
[9] K. Gawędzki and K. Rzążewski, No-go theorem for the superradiant phase transition without dipole approximation, Phys. Rev. A **23**, 2134 (1981).
[10] F. Dimer, B. Estienne, A. S. Parkins, and H. J. Carmichael, Proposed realization of the Dicke-model quantum phase transition in an optical cavity QED system, Phys. Rev. A **75**, 013804 (2007).
[11] K. Baumann, C. Guerlin, F. Brennecke, and T. Esslinger, Dicke quantum phase transition with a superfluid gas in an optical cavity, Nature (London) **464**, 1301 (2010).
[12] K. Baumann, R. Mottl, F. Brennecke, and T. Esslinger, Exploring Symmetry Breaking at the Dicke Quantum Phase Transition, Phys. Rev. Lett. **107**, 140402 (2011).
[13] P. Nataf and C. Ciuti, No-go theorem for superradiant quantum phase transitions in cavity QED and counter-example in circuit QED, Nat. Commun. **1**, 72 (2010).
[14] O. Viehmann, J. von Delft, and F. Marquardt, Superradiant Phase Transitions and the Standard Description of Circuit QED, Phys. Rev. Lett. **107**, 113602 (2011).
[15] C. Ciuti and P. Nataf, Comment on "Superradiant Phase Transitions and the Standard Description of Circuit QED", Phys. Rev. Lett. **109**, 179301 (2012).
[16] T. Jaako, Z.-L. Xiang, J. J. Garcia-Ripoll, and P. Rabl, Ultrastrong-coupling phenomena beyond the Dicke model, Phys. Rev. A **94**, 033850 (2016).
[17] M. H. Devoret, Quantum Fluctuations in Electrical Circuits, in *Proceedings of the Les Houches Summer School, Session LXIII*, edited by S. Reynaud, E. Giacobino, and J. Zinn-Justin (Elsevier, Amsterdam, 1997), Chap. 10, pp. 351–386.
[18] K. Hepp and E. H. Lieb, Equilibrium Statistical Mechanics of Matter Interacting with the Quantized Radiation Field, Phys. Rev. A **8**, 2517 (1973).
[19] J. L. van Hemmen and K. Rzążewski, On the thermodynamic equivalence of the Dicke maser model and a certain spin system, Phys. Lett. **77A**, 211 (1980).
[20] P. Nataf and C. Ciuti, Vacuum Degeneracy of a Circuit QED System in the Ultrastrong Coupling Regime, Phys. Rev. Lett. **104**, 023601 (2010).
[21] V. V. Ryazanov, V. A. Oboznov, A. Y. Rusanov, A. V. Veretennikov, A. A. Golubov, and J. Aarts, Coupling of Two Superconductors through a Ferromagnet: Evidence for a π Junction, Phys. Rev. Lett. **86**, 2427 (2001).
[22] C. Emary and T. Brandes, Quantum Chaos Triggered by Precursors of a Quantum Phase Transition: The Dicke Model, Phys. Rev. Lett. **90**, 044101 (2003).
[23] C. Emary and T. Brandes, Chaos and the quantum phase transition in the Dicke model, Phys. Rev. E **67**, 066203 (2003).
[24] See Supplemental Material at http://link.aps.org/supplemental/10.1103/PhysRevLett.117.173601, which includes Refs. [25,26], for additional discussion and detailed calculation.
[25] J. Keeling, Coulomb interactions, gauge invariance, and phase transitions of the Dicke model, J. Phys. Condens. Matter **19**, 295213 (2007).
[26] J. M. Knight, Y. Aharonov, and G. T. C. Hsieh, Are superradiant phase transitions possible?, Phys. Rev. A **17**, 1454 (1978).
[27] V. I. Emeljanov and Y. L. Klimontovich, Appearance of collective polarisation as a result of phase transition in an ensemble of two-level atoms, interacting through electromagnetic field, Phys. Lett. **59A**, 366 (1976).
[28] M. Yamanoi and M. Takatsuji, Influence of omitting the P^2 term in the multipole photon-matter Hamiltonian on the stability and propagation, in *Coherence and Quantum Optics IV: Proceedings of the Fourth Rochester Conference on Coherence and Quantum Optics*, edited by L. Mandel and E. Wolf (Plenum Press, New York, 1978), pp. 839–850.
[29] J. J. Hopfield, Theory of the Contribution of Excitons to the Complex Dielectric Constant of Crystals, Phys. Rev. **112**, 1555 (1958).
[30] C. Ciuti, G. Bastard, and I. Carusotto, Quantum vacuum properties of the intersubband cavity polariton field, Phys. Rev. B **72**, 115303 (2005).
[31] M. Bamba and T. Ogawa, Stability of polarizable materials against superradiant phase transition, Phys. Rev. A **90**, 063825 (2014).